Journal of Nuclear Materials 408 (2011) 142–152

Contents lists available at ScienceDirect

Journal of Nuclear Materials

journal homepage: www.elsevier.com/locate/jnucmat

A model for the normal stress dependence of intergranular cracking of irradiated 316L stainless steel in supercritical water

E.A. West *, G.S. Was

University of Michigan, 2355 Bonisteel Boulevard, Ann Arbor, MI 48109, United States

ARTICLE INFO

Article history:
Received 21 August 2010
Accepted 3 November 2010

ABSTRACT

The intergranular cracking behavior of irradiated 316L stainless steel in supercritical water (SCW) was found to be strongly dependent on the local grain boundary normal stress. Tensile specimens of 7 dpa proton irradiated 316L stainless steel were strained in 400 °C SCW to 2%, 5%, and 10% macroscopic plastic strain. The cracking behavior was characterized according to the distributions of cracked grain boundary plane surface trace inclinations to the tensile axis and the Schmid factors of the grains adjacent to the cracked boundaries. Cracks occurred preferentially along grain boundaries with trace inclinations perpendicular to the tensile axis and adjacent to grains with low Schmid factors. There was also a slight increase in cracking propensity for grain boundaries adjacent to grains with high Schmid factor mismatch. The normal stress dependence of intergranular cracking was confirmed by developing and applying the Schmid-Modified Grain Boundary Stress model which characterizes the normal stress acting on a grain boundary as a function of the inclination of the grain boundary plane to the tensile axis and the flow stress of the grain, as estimated from its Schmid factor. By applying this model, the Schmid factor dependence of intergranular cracking could be predicted from the distributions of cracked grain boundary trace inclinations to the tensile axis.

1. Introduction

Intergranular cracking and cavitation of metals are not equally likely at all grain boundaries. For example, they have been found to preferentially occur at randomly oriented high angle grain boundaries [1–3] and at grain boundaries oriented perpendicular to the tensile axis [4,5]. In this study, the influence of the grain-to-grain variations in deformation propensity on intergranular cracking is evaluated.

Deformation in polycrystalline materials is often a heterogeneous process [6]. Slip occurs primarily along the most densely packed planes and directions in the crystal, but the orientations of these slip systems and their ease of activation depend on their orientations with respect to the tensile axis. Slip systems with high Schmid factors, m, require less applied tensile stress to activate because they are oriented for maximum shear stress. The Schmid factor of a grain can be calculated from its most favorably oriented slip system as follows,

$$m = \cos\lambda \cos\phi \tag{1}$$

where λ is the angle between the slip direction and the tensile axis, and ϕ is the angle between the slip plane normal and the tensile axis. In the special case of a single crystal, the yield stress of the grain, σ_{y_g} can be expressed as a function of m and the critically resolved shear stress, τ_{CRSS},

$$\sigma_{y_g} = \frac{\tau_{CRSS}}{m} \tag{2}$$

Because of the higher yield strengths of grains with low Schmid factors, the stress distribution in an isotropic polycrystal cannot be uniform.

Experimental techniques are available to directly measure the plastic strain heterogeneities that develop in polycrystalline materials, and have demonstrated that grains with higher Schmid factors tend to experience higher levels of strain than those with low Schmid factors [7]. No techniques are currently available, however, to directly measure the stress fields in polycrystalline materials as they plastically deform, with finite element analysis being perhaps the most viable option to analyze local stresses. While finite element analysis offers the advantage of being able to account for the elevated levels of stress that may develop around geometrical or structural irregularities along grain boundaries such as near triple junctions or at sites of slip band intersection with grain boundaries [8], such modeling techniques cannot be used to evaluate the stress distributions over extensive areas of polycrystals. In the current study, over 4500 grains are analyzed, and the Schmid factor and inclination of the grain boundary plane surface trace with respect to the tensile axis will be used to

* Corresponding author. Tel.: +1 734 717 2824; fax: +1 734 763 4540.
E-mail address: eawest@umich.edu (E.A. West).

0022-3115/$ - see front matter © 2010 Elsevier B.V. All rights reserved.
doi:10.1016/j.jnucmat.2010.11.012

evaluate the local normal stress acting on the grain boundary by developing and applying the Schmid-Modified Grain Boundary Stress (SMGBS) model. In this way, the influence of the local grain boundary normal stress on the intergranular cracking behavior will be evaluated for an irradiated 316L stainless steel strained in a 400 °C SCW environment.

2. Experiment

2.1. Sample preparation

The chemical composition of the 316L stainless steel used in this study is given in Table 1. The as-received plate was annealed at 1100 °C for 20 min followed by an immediate water quench. The tensile specimens and spacing bars were fabricated through electrical discharge machining and had 2 mm × 2 mm square cross sections. The tensile specimens were machined such that the tensile direction was parallel to the rolling direction, and the specimen face parallel to the rolling surface was tracked for future crack analysis. The face of the spacing bar parallel to the rolling surface was also tracked for post-irradiation hardness measurements.

The specimens were mechanically polished with SiC abrasive paper to 4000 grit and subsequently electropolished in a 10% perchloric acid and 90% methanol solution to remove any residual damage induced by mechanical polishing. The specimens were electropolished at 30 V for approximately 30 s at a temperature of −50 °C.

2.2. EBSD analysis

Electron backscatter diffraction analysis (EBSD) analysis was performed on the gage surfaces of the tensile specimens with a Philips XL30FEG SEM equipped with a TexSEM Laboratories orientation imaging microscopy (OIM^{TM}) system. Four specimens were analyzed, and the cumulative scan areas included over 4500 grains. The OIM™ scans were performed with a step size less than one-tenth of the grain size with an accelerating voltage of 20 kV. The four corners defining each of the analyzed regions were marked with hardness indentations created with a 25 g load. The indents were used for ensuring proper sample alignment with the OIM™ system and as identifying marks for cracked boundary identification. The indentation area and deformation region surrounding the indent with a radius of three times the diagonal length of the indent were excluded from cracking analyses.

The Schmid factors of each of the grains in the scanned regions were determined by defining the 12 slip systems along the {1 1 1} planes in the ⟨1 1 0⟩ directions. The TSL OIM^{TM} Analysis version 5 software was then used to determine the Schmid factors of each of the 12 slip systems. The Schmid factor of the slip system with the highest resolved shear stress for the defined tensile direction was then reported as the Schmid factor of the grain. The EBSD data was processed through three cleanup procedures before generating Schmid factor maps of the analyzed regions. The first cleanup procedure identified points having a low confidence of being correctly indexed (confidence index of <0.1) and assigned those points the orientations of their neighboring points with the highest confidence indexes. The second procedure restricted the minimum grain size to twice the scan step size, and grains below this size were incorporated into surrounding grains. The final procedure determined the average orientation of the grain and assigned to all points within the grain the same "averaged" orientation. This procedure was performed to obtain the best indicator of the Schmid factor of the grain as a whole, and eliminated the slight variations in Schmid factor measurements in various regions of the grains.

Table 1
Chemical composition of 316L stainless steel (wt.%).

Alloy	Fe	C	Mn	P	Si	Ni	Cr	Mo	Cu	Co
316L	Bal.	0.022	1.86	0.03	0.51	10.12	16.62	2.06	0.24	0.05

2.3. Proton irradiations

The specimens were irradiated with 2 MeV protons to a dose of 7 dpa with the General Ionex Tandetron Accelerator at the University of Michigan Ion Beam Laboratory at the University of Michigan. The samples were loaded onto a custom designed copper stage, and thermal contact between the specimens and stage was achieved by placing thin sheets of indium foil in a shim beneath the specimens which became molten at the irradiation temperature. The temperature was monitored using a two-dimensional thermal imaging system and controlled to 400 ± 10 °C with a resistive cartridge heating and cooling lines that allowed air to flow through the back of the copper stage. The proton beam was 3 mm in diameter and it was raster-scanned over a 10 mm length of the specimens that was defined by a set of tantalum apertures. The temperature, stage current, and aperture current were recorded throughout the irradiation using a PC-based monitoring system.

The 2 MeV protons created a damage profile that extended to a depth of 20 μm into the sample substrate. In the plateau region of the damage peak, which extended to approximately 15 μm, the dose rate was approximately 10^{-5} dpa/s. The damage rate and profile were determined by performing a SRIM2006 [9] simulation with a displacement energy of 40 eV. Additional details regarding proton irradiation procedures at the University of Michigan can be found in other literature [10].

The proton irradiation increased the hardness of the specimens from 150 Hv to 380 Hv, which corresponded to an increase in yield strength of approximately 700 MPa [11]. Previous analysis of irradiated 316L specimens [12] showed that a 7 dpa proton irradiation resulted in the formation of dislocation loops and a low density of voids. The dislocation loops had an average diameter of 7 nm and were present at a density of 5.3×10^{22} m^{-3}. The void density was $<10^{20}$ m^{-3} and the few that were observed were approximately 2 nm in diameter. The irradiation depleted the chromium at the grain boundary from an enriched level of 19.1 wt.% in the unirradiated condition to 14.4 wt.% following the 7 dpa irradiation [11].

2.4. Constant extension rate tensile tests

The four tensile specimens underwent simultaneous constant extension rate tensile (CERT) tests in 400 °C SCW at a pressure of 24 MPa. The dissolved oxygen content of the water was <10 ppb and the conductivity was <0.10 μS/cm for the duration of the experiment. The samples were strained at a rate of 3×10^{-7} s^{-1}, and the experiment was interrupted at 2%, 5%, and 10% macroscopic plastic strain for cracking analysis. Measurements of the spacing of the hardness indents following each straining increment indicated that the plastic strains in the irradiated regions of the specimens were approximately 0.9%, 3.9%, and 8.0%, respectively. This plastic strain in the irradiated region was primarily the result of plastic deformation in the matrix, as the pseudo-strain induced by crack opening accounted for roughly 0.3%, 1.7%, and 7.8% of the plastic strain in the irradiated region.

After each straining increment, the specimens were analyzed at magnifications of 1000× with a JEOL JSM-6480 SEM, and all detectable cracks were analyzed. SEM images of the gage surfaces of the specimens were compared to the pre-irradiation OIM™ grain maps to determine the Schmid factors of both grains adjacent to the

cracked boundary. The inclination of the surface trace of each cracked grain boundary to the tensile axis was also measured. The trace inclination of each cracked grain boundary, θ, was measured from the line drawn between the triple junctions at either end of the cracked grain boundary as viewed from the specimen gage surface. If the crack did not extend the entire length of the grain boundary, the trace inclination was measured from the line drawn between either ends of the crack tip. At 2%, 5%, and 10% strain the numbers of cracked grain boundaries analyzed were 51, 238, and 448, respectively.

One of the four specimens was oxide stripped following crack analysis after each straining increment. This was done in order to make accurate measurements of the strain that occurred in the irradiated regions of the specimens and to characterize the extent of localized lattice rotation than developed during straining via EBSD analysis. The oxide stripping treatment was performed by submerging the specimens in a 100 g/l sodium hydroxide, 30 g/l potassium permanganate solution at 95 °C for 5 min followed by submersion in a 100 g/l ammonium oxalate solution at 95 °C for an additional 5 min. This treatment was performed a total of 3 times following each straining increment. The intergranular cracking behavior of the oxide stripped specimen was compared to that of the unstripped specimens, and it was determined that this treatment did not change the observed cracking correlations with Schmid factor or grain boundary inclination [11].

3. Results

The cracks that formed on the gage surfaces of the irradiated tensile specimens following straining in 400 °C SCW were primarily short and intergranular. The cracks widened with progressive straining, but generally did not show a strong tendency to propagate as illustrated in Fig. 1. The total numbers of cracked grain boundaries analyzed were 51, 238, and 448 at 2%, 5%, and 10% strain, respectively. The average number of cracked grain boundaries (defined as the regions between triple junctions) per continuous crack were 1.1, 1.4, and 1.6 at 2%, 5%, and 10% strain, respectively.

The cracks preferentially developed along grain boundaries that were perpendicular to the tensile axis as shown in Figs. 1 and 2. Following straining to 2%, there was a strong peak in the trace inclination distribution at 90°. This behavior continued with progressive straining, although the trace inclination distribution broadened substantially, and boundaries with trace inclinations as low as 15° were observed to crack. At 2%, 5%, and 10% strain, 90%, 82%, and 76% of the cracked boundaries had trace inclinations >60°.

The Schmid factor mismatch at each cracked grain boundary was determined by subtracting the Schmid factor of the grain with the lower Schmid factor from that with the higher Schmid factor. In this way, a *single* Schmid factor mismatch value was calculated for each cracked grain boundary. The Schmid factor mismatch crack distribution is shown in Fig. 3a where it can be seen that the distribution is strongly peaked at low Schmid factor mismatch values. In order to analyze this data in an unbiased manner, it is necessary to normalize the data to the total mismatch distribution in the alloy as a whole. This Schmid factor mismatch distribution, shown in Fig. 3b, was generated from the total distribution of Schmid factors in the alloy by assuming the grains were randomly distributed. The crack distribution was then normalized by dividing each bar corresponding to a certain Schmid factor mismatch bin by the value of the mismatch bin in the alloy as a whole. The resulting normalized distribution, Fig. 3c, shows a slight dependence on Schmid factor mismatch. While 24% of the total grain boundary population has

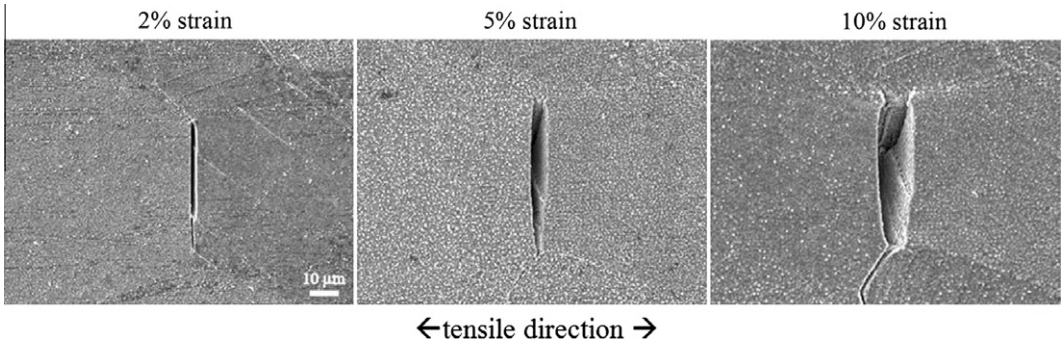

Fig. 1. Crack micrographs of 7 dpa proton irradiated 316L following straining to 2%, 5%, and 10% strain in 400 °C SCW.

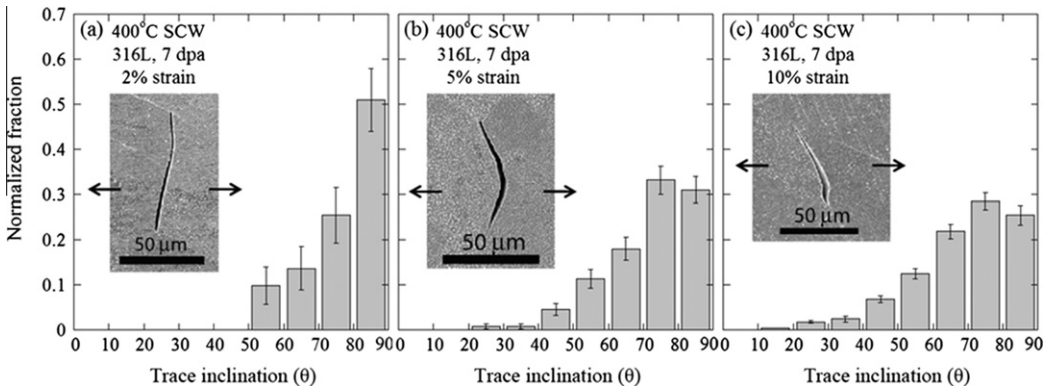

Fig. 2. Fraction of cracked grain boundaries with specified trace inclinations for 7 dpa proton irradiated 316L strained to (a) 2%, (b) 5%, and (c) 10% strain in 400 °C SCW.

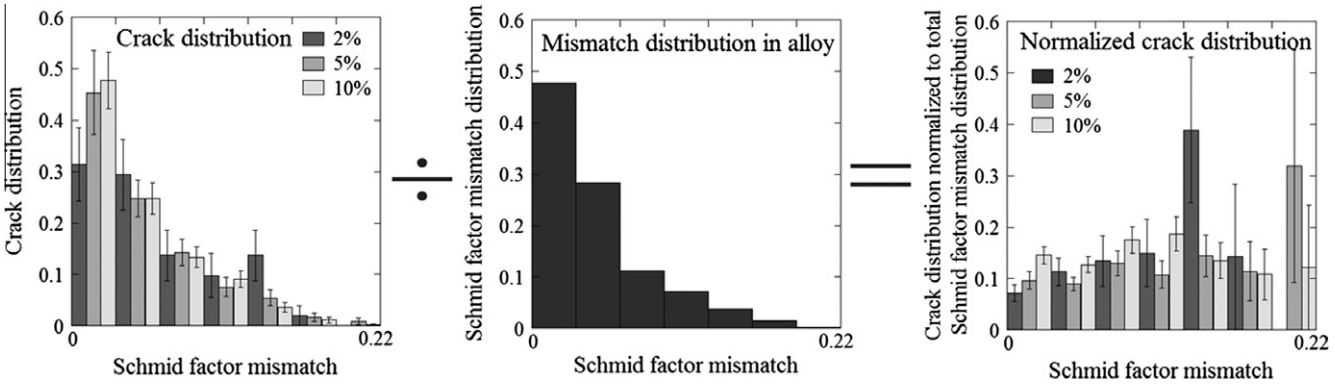

Fig. 3. Schmid factor mismatch crack distribution for 7 dpa proton irradiated 316L following straining to 2%, 5%, and 10% strain in 400 °C SCW. The crack distribution is normalized to the total mismatch distribution in the alloy and the resulting normalized cracked Schmid factor mismatch distribution is shown on the far right.

a mismatch of 0.07 or greater, 39%, 30%, and 27% of the intergranular cracks occur at locations exceeding this mismatch at 2%, 5%, and 10% strain, respectively.

In addition to evaluating the Schmid factor mismatch at the cracked grain boundaries, the Schmid factors of the grains adjacent to the cracks were also analyzed. As shown in Fig. 4, the crack distributions must again be normalized in order to view the data in an unbiased manner. In this case, the distribution of Schmid factors at the cracked grain boundaries, Fig 4a, is normalized to the Schmid factor distribution in the alloy, Fig. 4b, to yield the normalized crack distribution, Fig. 4c. The Schmid factors of both grains adjacent to each cracked grain boundary are included in these plots. Fig. 4 illustrates the importance of collecting large data sets. Even with the large sample areas analyzed, the error bars on the normalized data at the lower end of the Schmid factor range approach the limit of statistical significance.

The normalized crack distribution plots as a function of Schmid factor indicate that low Schmid factor grains promote intergranular cracking as shown in Fig. 5. At all levels of strain, the intergranular cracks preferentially form adjacent to grains with low Schmid factors. The strength of the correlation, however, weakens with progressive straining.

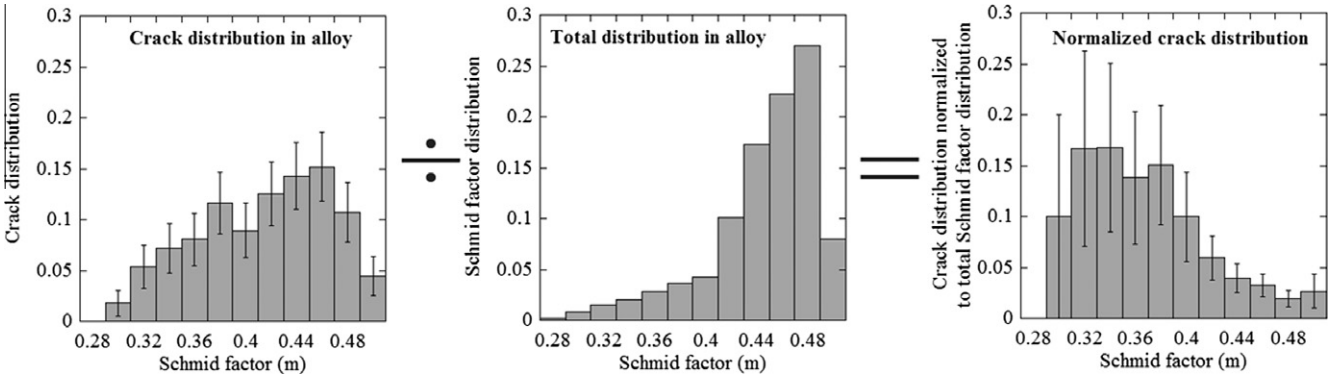

Fig. 4. Normalization procedure for analyzing the distributions of the Schmid factors of the grains adjacent to the cracked grain boundaries. The Schmid factors of both grains adjacent to the cracks are included in the distributions. The Schmid factor crack distribution is normalized to the total Schmid factor distribution in the alloy and the resulting normalized cracked Schmid factor distribution is shown on the far right.

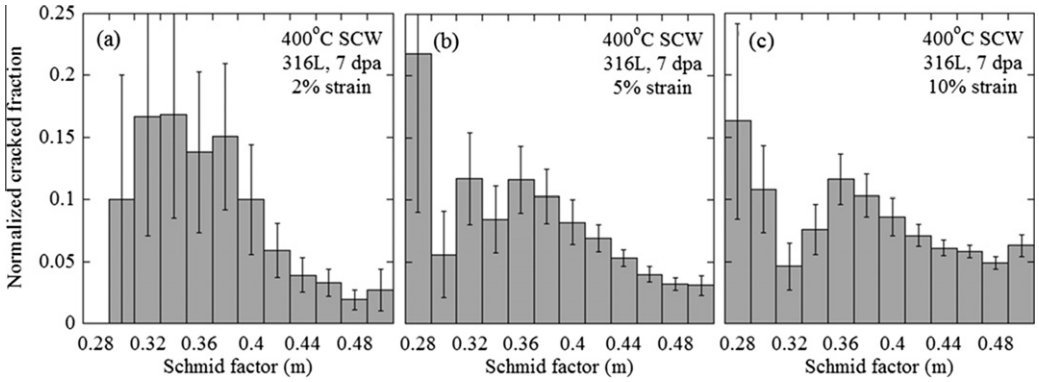

Fig. 5. Normalized fraction of cracked grain boundaries with specified Schmid factor pair types for 7 dpa proton irradiated 316L strained to (a) 2%, (b) 5%, and (c) 10% strain in 400 °C SCW.

4. Schmid-Modified Grain Boundary Stress (SMGBS) model

The preferential formation of intergranular cracks along grain boundaries perpendicular to the tensile axis and along grain boundaries adjacent to grains with low Schmid factors will be discussed in the context of the local grain boundary stress. It will be argued that the local grain boundary stress is influenced by both the inclination of the grain boundary plane to the tensile axis and the Schmid factor of the adjacent grain, which describes its propensity to deform. To explore the combined influence of the trace inclination and Schmid factor on the local grain boundary stress, the Schmid-Modified Grain Boundary Stress (SMGBS) model is proposed. This model is *not* intended to provide quantitative indicators of the stress acting on specific grain boundaries, rather it is intended to demonstrate that *the boundary to boundary variations in local stress are influence by the propensities of the grains to deform in addition to the inclination of the grain boundary plane to the tensile axis.*

It is noted that the SMGBS model does not account for the change in stress intensity at the crack tip as the crack progresses, which is widely recognized to influence crack growth. Therefore, this model is more applicable to the study of crack initiation than propagation. In this study, the crack propagation was minimal. The majority of the cracks analyzed at 2%, 5%, and 10% strain did not extend beyond a single grain boundary facet. Furthermore, the SMGBS model only considers one of the two grains adjacent to the grain boundary, and does not account for the local grain boundary geometries or the inhomogeneities in plastic deformation of polycrystals.

4.1. SMGBS model theory

The basic principle of the SMGBS model is that the stress acting on a grain boundary is dependent upon both the inclination of the grain boundary plane to the tensile axis and the deformation propensity of the grain adjacent to the boundary. The grain boundary plane inclination dependence of the normal stress will be discussed first. The normal stress acting on a grain boundary as the grain plastically deforms, σ_N, can be calculated as a function of the flow stress of the grain, σ_{f_g}, and the angle between the normal to the grain boundary plane and the tensile axis, α. σ_N is equal to the component of the axial load acting perpendicular to the grain boundary plane, f, divided by the surface area over which it is acting, a. f is the product of the tensile force acting on the grain, F_g, and $\cos(\alpha)$. The area over which f acts, a, is $A_g/\cos(\alpha)$ as illustrated in Fig. 6. Therefore, σ_N can be expressed as,

$$\sigma_N = \frac{f}{a} = \frac{F_g \cos\alpha}{A_g/\cos\alpha} \tag{3}$$

When the grain is deforming, the local tensile stress acting on the grain is equal to the flow stress of the grain, σ_{f_g}, which can be expressed as,

$$\sigma_{f_g} = \frac{F_g}{A_g} \tag{4}$$

Thus, σ_N can be expressed as,

$$\sigma_N = \sigma_{f_g}(\cos\alpha)^2. \tag{5}$$

Therefore, the maximum normal stress is achieved when the grain boundary plane is perpendicular to the tensile axis, $\alpha = 0°$. The value of σ_{f_g} is indicative of the propensity of the individual grain to deform, however, and is not identical for all grain orientations. The deformation behavior of polycrystalline materials is often discussed through (1) upper-bound or (2) lower-bound analyses which assume either (1) geometrically self-consistent deformation fields while stress is averaged over all grains, or (2) self-consistent internal stress fields with the strain averaged over all grains [13]. In this study, an isostrain assumption (that all grains in the polycrystal undergo the same shape change) will be applied to evaluate the local stresses acting on individual grain boundaries.

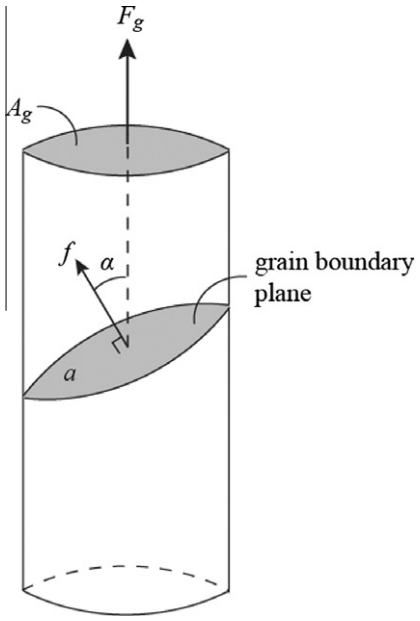

Fig. 6. Definition of variables for Eq. (3).

First, the yielding behavior of single crystals will be discussed in terms of their plastic anisotropies. An isolated grain will strain elastically until the resolved shear stress acting on the most favorably oriented slip system reaches the critically resolved shear stress, τ_{CRSS}, to cause slip according to Schmid's Law [14]. The yield stress of a single crystal is inversely proportional to the Schmid factor, m, of the most favorably oriented slip systems. The yield stress of an isolated grain, σ_{y_g}, can therefore be expressed as,

$$\sigma_{y_g} = \frac{\tau_{CRSS}}{m} \tag{6}$$

with smaller values of m indicating that more applied stress will be required to activate the slip system. Once plastic deformation commences, σ_{f_g} determines the strength of the grain and depends on the extent of strain hardening in the alloy.

4.2. SMGBS modeling approximations and assumptions

The previous section established that both the inclination of the grain boundary plane to the tensile axis and the flow stress of the adjacent grain influence the local stress on the grain boundary. The application of this theory to the current study presents challenges, however, as the values of α and σ_{f_g} are unknown. Therefore, assumptions and approximations will be applied to evaluate the local grain boundary stresses.

First, the value of α will be considered. Although the true value of α will remain unknown, the surface trace of the inclination of the grain boundary with respect to the tensile axis, θ, was measured experimentally. In order to determine α, it is necessary to define another angle, β, as the angle of rotation around the surface trace of the grain boundary plane as shown in Fig. 7. The reference orientation for β ($\beta = 0$) occurs when the grain boundary plane and specimen surface are coincident with the front of the specimen. Therefore, the surface trace vector, v_1, and the angles θ and β fully define the grain boundary plane orientation. In order to obtain a

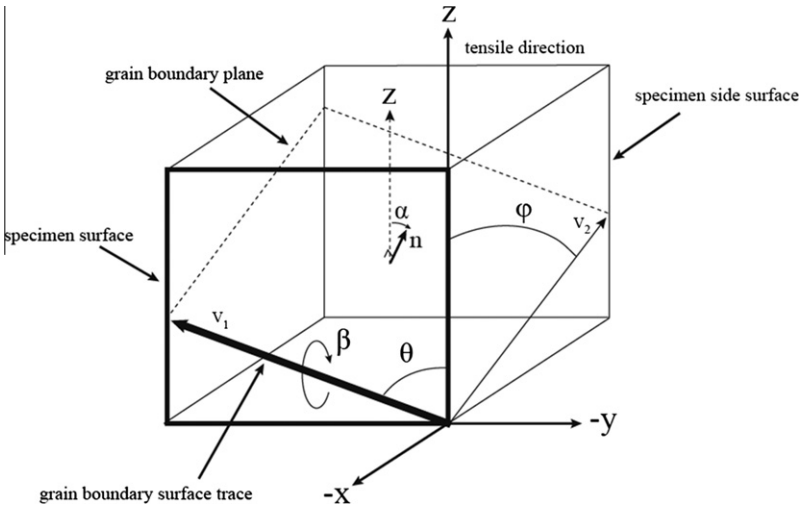

Fig. 7. Illustration of grain boundary geometry, and definition of variables used in this study: n is the normal to the grain boundary plane, α is the angle between the normal to the grain boundary plane and the tensile direction, φ is the angle between the tensile direction and the trace of the grain boundary on the side surface of the specimen, θ is the trace inclination, and β is the angle of rotation about the grain boundary surface trace vector.

more simplified expression for α, a fourth variable, φ, will be defined. In accordance with the work of Alexandreanu [15], φ is the angle between the tensile direction and the grain boundary plane trace vector, v_2, on the side surface perpendicular to the sample surface as shown in Fig. 7. The cross product of the vectors, v_1 and v_2, defines the normal to the grain boundary plane which can be used to calculate α,

$$\alpha = \arccos\left(\sqrt{\frac{1}{\tan^2\varphi}+\frac{1}{\tan^2\theta}+1}\right)^{-1} \tag{7}$$

where

$$\varphi = \arctan\sqrt{\frac{\frac{1}{\cos^2\beta}-1}{\frac{1}{\tan^2\theta}+1}} \tag{8}$$

and the full derivations are included in other literature [11]. Measurements of the grain boundary surface traces on the specimen surface confirmed that θ was approximately random, and the values of β are all assumed to be equally likely. Thus, α can be calculated as a function of θ and β with all values of θ and β assumed to be equally likely.

In addition to α, the values of σ_{f_g} for the individual grains within a polycrystalline material are also unknown. Irradiation of 316L to 7 dpa will significantly reduce the strain hardening compared to that experienced in an unirradiated alloy [16,17]. The strain hardening may therefore be approximated as zero for this material, making $\sigma_{f_g} = \sigma_{y_g}$. It is important to consider that this assumption is generally applicable to highly irradiated stainless steels where the strain hardening is often on the order of only 10% of the true fractures stress, but is not justifiable for unirradiated stainless steels where the strain hardening may be on the order of 70–80% of the true fracture stress [17].

The single crystal assumption will also be applied, in which $\sigma_{y_g} \propto \frac{1}{m}$ (and therefore $\sigma_{f_g} \propto \frac{1}{m}$). While this equation is applicable to an isolated grain, it may be argued that it is not perfectly applicable to a polycrystalline material because the stress fields in a polycrystalline material will always be multiaxial even when a uniaxial load is applied to the specimen as a result of the deformation restrictions imposed by surrounding grains. It was observed, however, that only a single slip plane was active in the majority of the grains, which meant that a maximum of two independent slip systems were active. It was also observed that the slip planes that contained the most favorably oriented slip systems nearly always activated. This indicates that any multiaxial loading that may be occurring is generally not great enough in the current study to overpower the ability to predict whether or not the most favorably oriented slip system activates as determined from the Schmid factor calculation.

Finally, it will be assumed that the yield stress, σ_y, and flow stress, σ_f, of the polycrystal are equal and proportional to the average Schmid factor of the polycrystal, m_{avg}, which was 0.45 for 316L,

$$\sigma_f = \sigma_y \propto \frac{1}{m_{avg}} \tag{9}$$

Therefore, σ_{f_g} may be expressed as,

$$\sigma_{f_g} = \sigma_f \frac{m_{avg}}{m_g} \tag{10}$$

and Eq. (5) may be rewritten as,

$$\sigma_N = \sigma_f \frac{m_{avg}}{m_g}(\cos\alpha)^2 \tag{11}$$

Finally, by setting the flow stress equal to 1, the normalized effective normal stress acting on the grain boundary, ${}^*\sigma_N$, can be expressed as,

$${}^*\sigma_N = \frac{0.45}{m_g}(\cos\alpha)^2 \tag{12}$$

4.3. Generation of SMGBS model curves

It was shown through Eqs. (7), (8), and (12) that ${}^*\sigma_N$ can be calculated as a function of three variables, m_g, θ, and β. To illustrate the normal stress dependence on these parameters, ${}^*\sigma_N$ curves are plotted as a function of θ for different values of m_g and β in Fig. 8. It can be seen from Fig. 8 that ${}^*\sigma_N$ is maximized when the Schmid factor is at its minimum value, $m_g = 0.27$, and $\theta = \beta = 90°$ ($\alpha = 0$). Under these conditions, ${}^*\sigma_N = 1.67$, or 167% of σ_f.

It is proposed here that the propensity for intergranular cracking is not necessarily linearly proportional to the stress acting on the grain boundary, but instead requires a critical threshold stress. The assumed existence of a threshold stress is based on the results of Alexandreanu, where it was observed that the intergranular cracking propensity as well at the grain boundary deformation

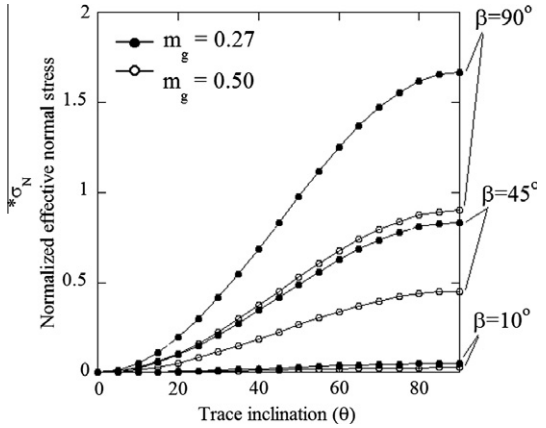

Fig. 8. Normalized effective normal stress as a function of trace inclination to the tensile axis, θ, for specific values of m_g and β.

propensity of Ni–16Cr–9Fe appeared to require a threshold shear stress [15,18]. The likelihood that the stress acting on a grain boundary is above a critical effective normal stress (CNS), for a given value of θ can be determined from the number of SMGBS model points above the threshold stress. Consider the weighted number of points above a CNS value for a given value of θ, WN_θ. The WN_θ values are calculated by summing all of the weighted model points which exceed a specified critical stress value for each value of θ. The SMGBS model curve generation procedure is illustrated in Fig. 9, and the summation is described with the following equations,

$$WN_\theta = \sum_{\beta=0}^{\beta=90} \sum_{m=0.27}^{m=0.50} N_{>\mathrm{CNS}}(\theta, \beta, m) \tag{13}$$

where

$$N_{>\mathrm{CNS}} = \begin{cases} 0 & \text{if } {}^*\sigma_N(\theta,\beta,m) \le \mathrm{CNS} \\ f_\beta f_m & \text{if } {}^*\sigma_N(\theta,\beta,m) > \mathrm{CNS} \end{cases} \tag{14}$$

f_β is the fraction of boundaries with the specified degree of rotation about v_1 (with all angles being equally likely), and f_m the fraction of grains with the specified Schmid factor, i.e. 0.2% of the grains have Schmid factors of 0.28 so $f_{0.28} = 0.002$. The WN_θ value can be calculated for each value of θ (0–90°) to generate a smooth WN_θ versus θ curve. The sparse population of grains with extremely low Schmid factors is reflected in Fig. 9. Although it can be seen that grains with Schmid factors of 0.27 are capable of exceeding the CNS value of 0.80 at trace inclinations as low as 45°, no grains with Schmid factors of 0.27 were found in the 6000 grains analyzed. Therefore, their contribution to the SMGBS model curve as a function of θ is zero following the weighting procedure.

In order to compare the SMGBS model dependence of θ to the crack dependence of θ (which is always normalized to 1), this model curve is also normalized. Thus, regardless of the number of SMGBS model points above the critical stress, the area under the SMGBS model curve is always constant. As the CNS value is decreased, the inflection point of the curve moves to lower values of θ, and as the CNS value increases, the peak in the SMGBS model curve at $\theta = 90°$ strengthens. SMGBS model curves can be generated as a function of any one of the three effective normal stress parameters, θ, m_g, or β, by summing the weighted number of modeling points above the CNS value for each value of θ, m_g, or β.

4.4. Alternative method of plotting SMGBS model curves

An alternative method of generating SMGBS model curves that will be used in a separate paper analyzing grain boundary strain incompatibilities [19] will be described in this section. Rather than

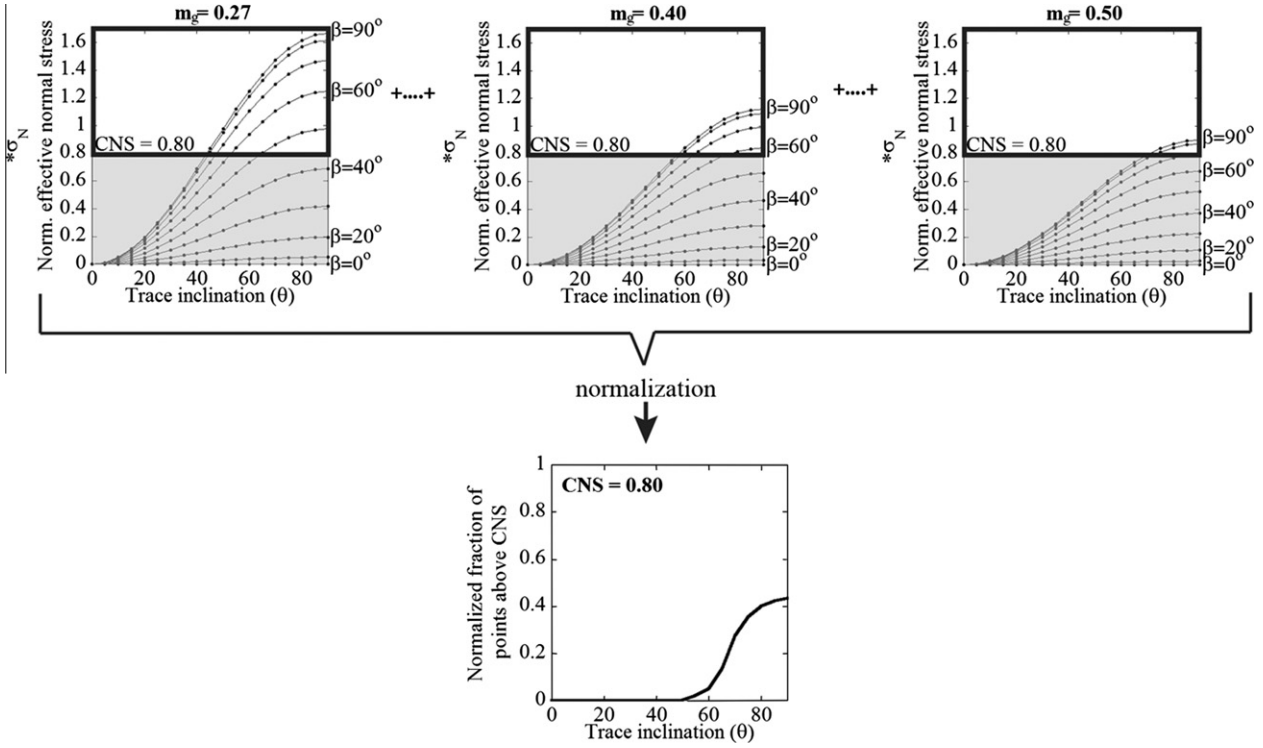

Fig. 9. Illustration of the procedure used to generate the SMGBS model curves. The modeling points with ${}^*\sigma_N(\theta,\beta,m_g) > \mathrm{CNS}$ are weighted according to the m_g and β populations, summed, and then the distribution is normalized to generate the final SMGBS model curve. In the current experiment, none of the 6000 grains analyzed to generate Schmid factor distributions had Schmid factors of 0.27. Therefore, the contribution of such low Schmid factor grains are eliminated during the weighting procedure and the final SMGBS model curve only exceeds zero at trace inclinations of 50° and above.

performing the final normalization treatment, the weighted fraction of SMGBS modeling points either above or below the CNS value can be determined as a function of any one of the three model variables (θ, m_g, or β). Using this method, the model curve value as a function of any one of the three variables will have values ranging between 0 and 1. This method of generating SMGBS model curves is applicable to situations in which the probability of an events occurring, such as slip continuity [19], is plotted as a function of one of the SMGBS model variables.

4.5. Application of SMGBS model to cracking data

The tendency of the intergranular cracks to occur along grain boundaries with trace inclinations perpendicular to the tensile axis and along grain boundaries adjacent to grains with low Schmid factors suggests that the local normal stress acting on the grain boundary may be influencing the cracking propensity. This hypothesis will be evaluated by applying the SMGBS model to the crack distributions as a function of trace inclination and Schmid factor.

The CNS values that result in the best fits to the cracked trace inclinations will be reported here. For each crack distribution, the CNS value reported is that which maximized the portion of the SMGBS model curve that fit the crack distribution. As shown in Fig. 10, as the strain increases from 2% to 5% to 10%, the CNS value that results in the best fit between the SMGBS model curves and the experimental data decreases from 0.92 to 0.67 and finally 0.57. The decrease in the CNS value may be an artifact of the change in stress intensity at the crack tip as it grows, which is not accounted for in the SMGBS model. It could also be indicative of a decrease in the intergranular cracking resistance of the grain boundary as corrosion occurs and damage accumulates near the grain boundaries with progressive straining. Using these same CNS values, SMGBS model curves were generated as a function of the Schmid factor. As shown in Fig. 11, the experimental data agree relatively well with the SMGBS model predicted dependence of cracking on Schmid factor. It can be seen that, as strain increases, the Schmid factor dependence of the cracking behavior decreases. This is also predicted by the model, in that, as the CNS decreases, the Schmid factor dependence of the SMGBS model curve weakens.

These findings suggest that the boundary to boundary variations in normal stress, as predicted by the trace inclination and Schmid factor, strongly influence the cracking propensities of the individual grain boundaries. One of the assumptions of the SMGBS model is that the stress acting on a grain boundary for a given value of β is always proportional to $1/m_g$. Therefore, the influence of the Schmid factor of the grain on the stress on the adjacent grain boundary will always be greater when the normal stress acting on the grain boundary is higher, i.e. for smaller values of α (larger values of θ and β). Therefore, as the CNS value decreases, the relative influence of the Schmid factor on the normal stress decreases. The fact that the cracking data also exhibit this same behavior thus supports the modeling assumptions.

It is acknowledged here, however, that the true normal stress acting on a grain boundary should be a function of the deformation propensities of both grains adjacent to the boundary. The model, however, only considers one of the two grains. Full analysis of the elastic and plastic deformation behaviors between adjacent grains at their interface is beyond the scope of this paper. If a sim-

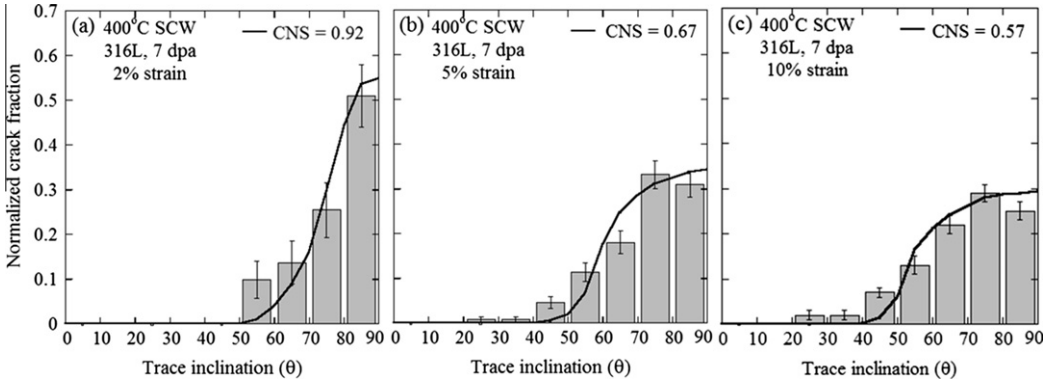

Fig. 10. Distributions of trace inclinations for intergranular cracks on 7 dpa proton irradiated 316L following straining in 400 °C SCW to (a) 2%, (b) 5%, and (c) 10% strain. The SMGBS model curves for the CNS values indicated are shown with solid black lines.

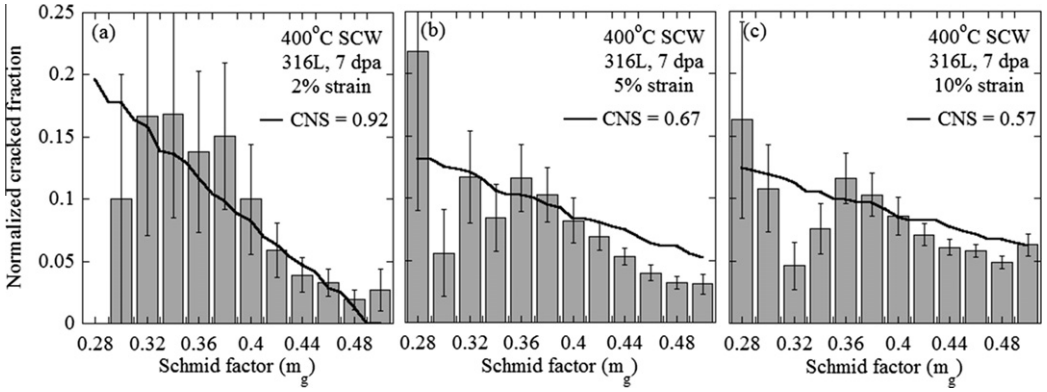

Fig. 11. Normalized cracked grain boundary fractions as a function of the Schmid factors of the grains adjacent to the boundary. The solid black curves indicate the SMGBS model fit to the trace inclination data at (a) 2%, (b) 5%, and (c) 10% strain with corresponding CNS values of 0.92, 0.67 and 0.57, respectively.

ple assumption was applied, however, that the tensile stress acting on the grain boundary were the average of the flow stresses of the adjacent grains, Eq. (12), could be modified to yield,

$$^{*}\sigma_N = \frac{1}{2}\left(\frac{0.45}{m_{g1}} + \frac{0.45}{m_{g2}}\right)(\cos\alpha)^2, \quad (15)$$

where m_{g1} and m_{g2} are the Schmid factors of both grains adjacent to the boundary. Under this assumption, the maximum and minimum normalized stresses would remain the same. Application of this equation to the experimental results, however, would require additional normalization treatments to account for the probabilities of grains with each Schmid factor value being adjacent to one another.

5. Discussion

The cracking results in this study will be discussed in the context of potential creep crack mechanisms. The SCW environment is considered important, as it increased the crack density of the irradiated 316L stainless steel by a factor of 18 at 5% strain when compared to results from a parallel study conducted in a 400 °C argon environment [11]. Although the SCW environment greatly enhanced intergranular cracking, however, it was not essential to crack nucleation. Creep is widely believed to influence intergranular cracking in high temperature environments through mechanisms such as grain boundary deformation or sliding [15,20], grain boundary void formation promoted by power law creep [21], or vacancy diffusion ahead of the crack tip [22]. Furthermore, similar cracking morphologies are observed from CERT experiments in SCW and creep experiments in air, as shown in Fig. 12. In both (a) and (b) the cracks are primarily short, intergranular, and oriented perpendicular to the tensile direction.

The distribution of cracked grain boundary inclinations has been shown to be dependent upon alloy [11], test temperature and irradiation [23], and strain rate [24]. The alloy, temperature, and irradiation dependence is shown in Fig. 13. It can be seen that a decrease in temperature from 500 °C to 400 °C results in a broadened distribution of trace inclinations, Fig. 12a and b. Depending on the alloy, irradiation may either result in a broadening of the trace inclination distribution as shown for 316L stainless steel in Fig. 12c and d, or the development of a peak at trace inclinations expected to experience maximum shear stress around 45° as shown for nickel-base alloy 690 in Fig. 12e and f. It can be seen from the development of peaks in the inclination distributions near 45° in Fig. 12f and h that nickel-base alloys (690 and 625) appear to have a stronger propensity for crack formation along grain boundaries with high shear stress than 316L.

The temperature dependence of the cracked trace inclination distribution could be the result of the increasing role of creep in the deformation behavior as the temperature increases as well as the decreasing strength of grain boundaries above the equicohesive temperature. Irradiation damage increases the strength, and therefore the stress experienced in such materials as they deform. As previously reported, the 7 dpa proton irradiation of 316L increased the yield strength by approximately 700 MPa. The presence of irradiation induced defects including dislocation loops and voids in the matrix would likely decrease the creep response of the material in post-irradiation straining experiments as a result of there being high densities of obstacles to pin dislocations. Furthermore, radiation induced segregation at grain boundaries may increase the susceptibility of the alloy to intergranular corrosion and/or decrease the cohesive strength of the grain boundary.

The development of intergranular cracks along grain boundaries that are perpendicular to the tensile axis is often observed [8,25,26], although the mechanism of crack nucleation is not always clear. Intergranular creep fracture is often characterized as wedge-type cracks or r-type cracks or cavities. While there is nearly universal support for the nucleation of wedge-type cracks due to the inability to accommodate grain boundary sliding, the mechanism for the nucleation of r-type cavities is still a subject of debate. Grain boundary sliding is often stated to be a key contributor to cavity formation, although in a more localized region for r-type cavities [25]. Grain boundary sliding, however, is expected to occur preferentially along boundaries oriented for maximum shear stress ($\alpha = 45°$). Therefore, the consistent observations of r-type (and sometimes wedge-type) cavity formation along boundaries perpendicular to the tensile axis appears contradictory, as it suggests normal rather than shear stress dependence.

While no consensus has been reached on this apparent discrepancy, some potential reasons have been discussed. Nucleation of cavities may occur thermally through condensation of vacancies on stressed surfaces, or as a result of dislocation pileup at grain boundaries. Dyson and McLean [27] proposed a theory of cavity nucleation that was later built upon by Dyson [28], that grain boundary decohesions develop athermally by dislocation pile up at obstacles, but that the only decohesions that develop into cavities by vacancy absorption are those with radii greater than a critical value that is dependent on the local steady state tensile stress. Because the critical cavity size would be small for grain boundaries with high normal stresses, more cavities would develop along

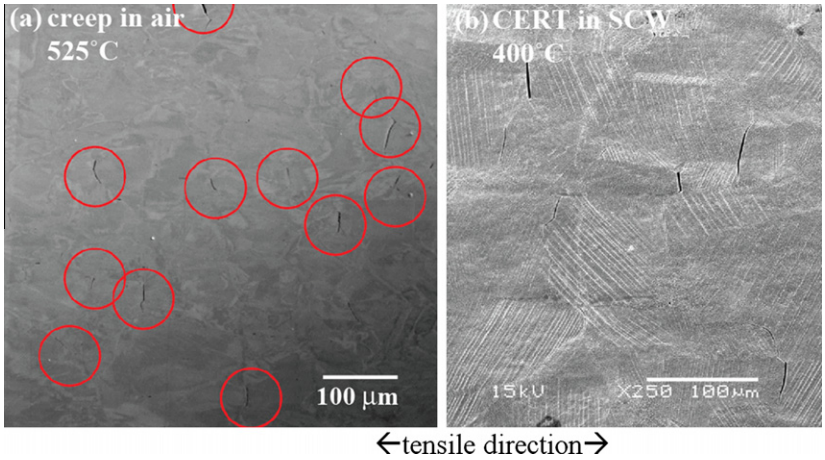

Fig. 12. (a) Intergranular fracture observed on 316 stainless steel following creep test in air [20] and (b) intergranular cracks on gage surface of 7 dpa proton irradiated tensile specimen strained to failure in 400 °C SCW [29].

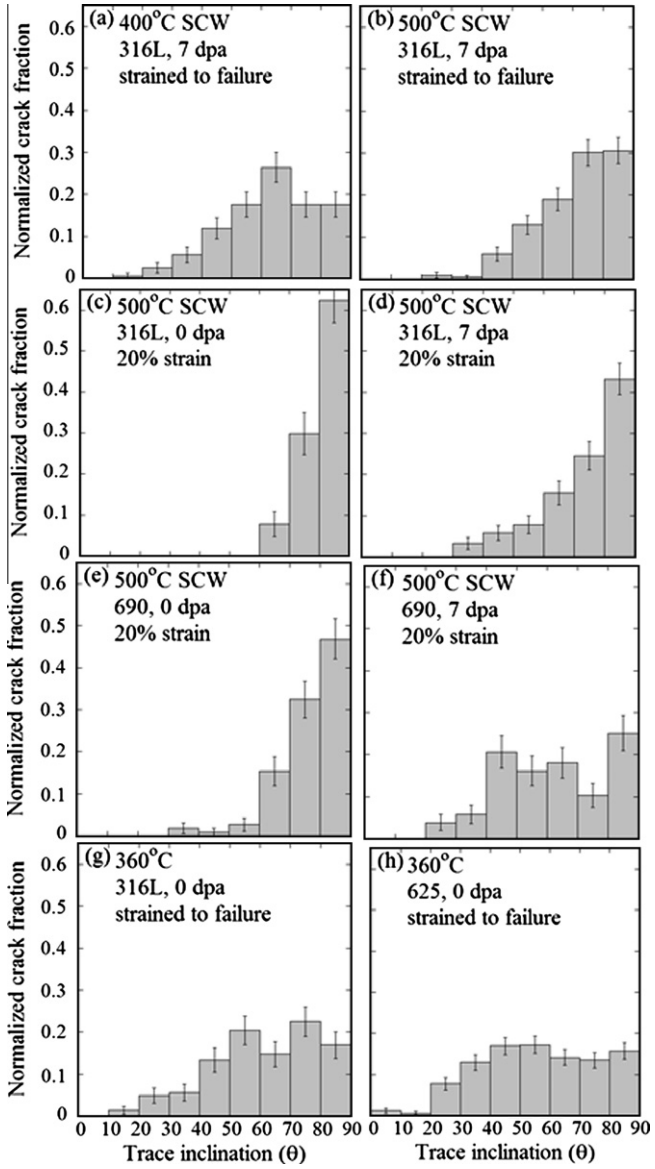

Fig. 13. Influence of (a) and (b) temperature, (c)–(f) irradiation, and (e)–(h) alloy on trace inclination dependence of intergranular cracking of austenitic alloys in high temperature aqueous environments. These measurements were collected from micrographs borrowed from other researchers from previous experiments [30,31], but this analysis was performed independently.

grain boundary planes perpendicular to the tensile axis. The dislocation channel step heights observed in the current study at times exceeded 1 μm, which results in substantial amounts of deformation at grain boundaries from dislocation pileup. Cracks were often not visible at such locations, however, indicating that factors other than the local strain influenced the propensity for crack formation. Courtney has also argued [25] that crack growth rates may be greater along grain boundaries perpendicular to the tensile axis. Therefore, although grain boundary sliding may induce either wedge-type or r-type cracking along grain boundaries with high shear stresses, the only cracks that will be detectable will be those that have the greatest propensity to grow. In the current study, cracks were only detected if they were at least 1–2 μm in length, whereas newly nucleated cavities are often only about 2–5 nm in size [8]. The measurements in the current study, therefore, are influenced by growth propensity as suggested by Dyson [28]. The observation that cracks develop along certain boundaries, however, indicates that they must have nucleated there as well. Therefore, the Schmid and trace inclination dependence of the cracking may either be the result of the normal stress dependence of crack nucleation, crack growth, or both phenomena.

6. Conclusions

The development of intergranular cracks on proton irradiated 316L stainless steel in 400 °C SCW is strongly dependent on the local grain boundary normal stress. This behavior was verified by developing and applying the SMGBS model which determines the effective normal stress acting on the grain boundary as a function of the inclination of the grain boundary plane to the tensile axis and the flow stress of the grain, as estimated from the Schmid factor of the grain. The SMGBS model predicted the Schmid factor dependence of IG cracking behavior on the trace inclination of cracks on the gage surface of the alloy in good agreement with measurement. The normal stress dependence of the cracking may either be a result of a higher propensity for intergranular crack nucleation on highly stressed surfaces, or the greater propensity for intergranular cracks to grow along boundaries experiencing high normal stresses.

Acknowledgements

The authors wish to thank the staff of the Michigan Ion Beam Laboratory, Ovidiu Toader and Fabian Naab, for use of the proton irradiation facilities and their assistance with the irradiations. The CERT tests were conducted in the Irradiated Materials Testing Laboratory and the manager, Alexander Flick is greatly acknowledged for his assistance in the laboratory. Reliable support of the EBSD equipment was provided University of Michigan Electron Microbeam Analysis Laboratory staff. This research was supported by the US Department of Energy, NERI award #DE-FC07-05ID14664 for Project Number 05-151.

References

[1] D.C. Crawford, G.S. Was, Metall. Trans. 23A (1992) 1195.
[2] B. Alexandreanu, B. Capell, G.S. Was, Mater. Sci. A 300 (2001) 94.
[3] E.A. West, G.S. Was, J. Nucl. Mater. 392 (2009) 264.
[4] M.E. Kassner, T.A. Hayes, Int. J. Plasticity 19 (2003) 1715.
[5] C. Gandhi, R. Raj, Metall. Trans. 12A (1981) 515.
[6] The Inhomogeneity of Plastic Deformation: Papers Presented at a Seminar of the American Society for Metals, American Society for Metals, Metals Park, Ohio, 1973.
[7] E. Heripre, M. Dexet, J. Crepin, L. Gelebart, A. Roos, M. Bornert, D. Caldemaison, Int. J. Plasticity 23 (2007) 1512.
[8] J. Čadek, Creep in Metallic Materials, Elsevier, Amsterdam, 1988.
[9] J.F. Ziegler, SRIM 2006, IBM Corporation, Yorktown, NY, 2006.
[10] G. Gupta, Z. Jiao, A.N. Ham, J.T. Busby, G.S. Was, J. Nucl. Mater. 351 (2006) 162.
[11] E.A. West, Influence of Local Stress and Strain on Intergranular Cracking of 316L Stainless Steel in Supercritical Water, University of Michigan, Ph.D. Thesis, Ann Arbor, MI, 2010.
[12] E.A. West, S. Teysseyre, Z. Jiao, G.S. Was, Influence of irradiation induced microstructure on the stress corrosion cracking behavior of austenitic alloys in supercritical water, in: Proc. 13th Int. Conf. on Environ. Degrad. in Nucl. Power Syst., Canadian Nuclear Society, Whistler, BC, vol. 2, 2007, p. 748.
[13] W.F. Hosford, The Mechanics of Crystals and Textured Polycrystals, Oxford University Press, New York, 1993.
[14] E. Schmid, Zeitschrift fuer Electrochemie und Angewandte Physikalische Chemie 37 (1931) 447.
[15] B. Alexandreanu, Grain Boundary Deformation-Induced Intergranular Stress Corrosion Cracking of Ni–16Cr–9Fe in 360 °C Water, University of Michigan, Ph.D. Thesis, Ann Arbor, MI, 2002.
[16] G.S. Was, Fundamentals of Radiation Materials Science. Metals and Alloys, Springer, Berlin, 2007.
[17] T.S. Byun, K. Farrell, E.H. Lee, J.D. Hunn, L.K. Mansur, J. Nucl. Mater. 298 (2001) 269.
[18] B. Alexandreanu, G.S. Was, Corrosion 59 (2003) 705.
[19] E.A. West, G.S. Was, Strain incompatibilities and their role in intergranular cracking of irradiated 316L stainless steel, J. Nucl. Mater., submitted for publication.
[20] K. Arioka, T. Yamada, T. Terachi, R.W. Staehle, Corrosion 62 (2006) 74.

[21] G.S. Was, J.K. Sung, T.M. Angeliu, Metall. Trans. 23A (1992) 3343.
[22] K. Arioka, T. Yamada, T. Terachi, T. Miyamoto, Corrosion 64 (2008) 691.
[23] E.A. West, Z. Jiao, G.S. Was, Influence of Taylor factor on IASCC in SCW and simulated BWR environments, in: Proc. 14th Int. Conf. on Environ. Degrad. in Nucl. Power Syst., Virginia Beach, VA. (2010) 1690.
[24] R.W. Evans, B. Wilshire, Creep of Metals and Alloys, Institute of Metals, London, 1985.
[25] T.H. Courtney, Mechanical Behavior of Materials, McGraw-Hill, Boston, 2000.
[26] G.E. Dieter, Mechanical Metallurgy, third ed., McGraw-Hill, New York, 1986.
[27] B.F. Dyson, D. McLean, Metal. Sci. 11 (1977) 37.
[28] B.F. Dyson, Continuous.Cavity. Nucleation, Creep. Fracture, Scripta Metall. 17 (1983) 31.
[29] G.S. Was, R. Zhou, E.A. West, Z. Jiao, Intergranular cracking behavior of irradiated austenitic alloys in supercritical water, in: Proc. 14th Int. Conf. on Environ. Degrad. in Nucl. Power Syst., Virginia Beach, VA. (2010) 1679.
[30] R. Zhou, E.A. West, Z. Jiao, G.S. Was, J. Nucl. Mater. 395 (2009) 11.
[31] P. Ampornrat, Intergranular Cracking of Austenitic Alloys in 360 °C Water – Personal Communication, Ann Arbor, MI, 2009.